Pharmacology Research & Perspectives

ORIGINAL ARTICLE OPEN ACCESS

Glutathione Decreases Parkinsonism-Induced Ferroptosis and Oxidative Stress Through the Inhibition of the TRPM2 Channel in Neuronal Cells

Elif Güzel[1,2,3] | Ayşe Arzu Sayın Şakul[1,3] | Mustafa Nazıroğlu[4,5,6]

[1]Department of Medical Pharmacology, Faculty of Medicine, Istanbul Medipol University, Istanbul, Türkiye | [2]Department of Medical Pharmacology, Institute of Health Sciences, Istanbul Medipol University, Istanbul, Türkiye | [3]Research Institute for Health Sciences and Technologies, Istanbul Medipol University, Istanbul, Türkiye | [4]Department of Biophysics, Faculty of Medicine, Suleyman Demirel University, Isparta, Türkiye | [5]Neuroscience Research Center, Suleyman Demirel University, Isparta, Türkiye | [6]BSN Health, Analyses, Innovation, Consultancy, Organization, Agriculture, Industry and Trade LTD, Isparta, Türkiye

Correspondence: Mustafa Nazıroğlu (mustafanaziroglu@sdu.edu.tr)

Received: 10 February 2025 | **Revised:** 15 April 2025 | **Accepted:** 15 April 2025

Funding: This work was supported by the Scientific Unit (BAP) of Istanbul Medipol University (Project Numbers: BAP-2023_22 and BAP-2023_23). The owner of the projects is Dr. Ayşe Arzu ŞAKUL.

Keywords: ferroptosis | glutathione | Parkinson's disease | SH-SY5Y cell death | TRPM2 channel

ABSTRACT

Parkinson's disease (PD) is the most prevalent neurodegenerative disease. Previously, it was believed that aberrant iron metabolism, leading to ferroptosis due to glutathione (GSH) depletion, excessive Ca^{2+} influx, mitochondrial (mROS), and cytosolic (cROS) free reactive oxygen species in the brain, was a contributing factor to PD. ADP-ribose (ADPR), mROS, and cROS activate the TRPM2 cation channel. It is yet unclear how TRPM2 contributes to the development of neuronal damage induced by the rise in ferroptosis in PD. Our aim in this study was to examine the function of TRPM2 and the protective effect of GSH in the dopaminergic human SH-SY5Y neuronal cells that had been exposed to 1-methyl 4-phenylpyridinium (MPP) to produce parkinsonism. The SH-SY5Y cells were divided into six groups: control, MPP, MPP + erastin, MPP + erastin + ferrostatin-1, MPP + erastin + glutathione (GSH), and MPP + erastin + TRPM2 blocker (ACA). In the MPP and MPP + erastin groups, the concentrations of Ca^{2+}, ADPR-induced TRPM2 current density, mitochondrial membrane dysfunction, mROS, cROS, lipid peroxidation, mitochondrial Zn^{2+}, cytosolic Zn^{2+}, and cytosolic Fe^{2+} were increased, although glutathione peroxidase, GSH, cell viability, and cell number were decreased. The changes were higher in the MPP + erastin group than in MPP group only. However, their concentrations were modulated by the changes in the MPP + erastin + ferrostatin-1, MPP + erastin + GSH, and MPP + erastin + ACA groups. In conclusion, the increase in death and ferroptosis in parkinsonism (MPP)-induced SH-SY5Y cells was attributed to TRPM2 activation. By regulating cytosolic oxidant/antioxidant balance, GSH regulates TRPM2 channel activity and lowers neuronal death and ferroptosis.

Abbreviations: 2-APB, 2-aminoethoxydiphenyl borate; ACA, N-(p-amylcinnamoyl)anthranilic acid; a.u, arbitrary unit; $c[Ca^{2+}]_c$, cytosolic free Ca^{2+} concentration; $c[Fe^{2+}]_c$, cytosolic free Fe^{2+} concentration; CGCC, chemical-gated calcium channels; cROS, cytosolic reactive oxygen species; $c[Zn^{2+}]_c$, cytosolic free Zn^{2+} concentration; Erst, erastin; Ferr1, ferrostatin 1; GSH, glutathione; GSH-Px, glutathione peroxidase; LPO, lipid peroxidation; LSM 800, laser scan confocal microscope; mDYS, mitochondrial membrane dysfunction; MiTr, Mito tracker red; MPP, 1-methyl-4-phenylpyridinium; mROS, mitochondrial reactive oxygen species; PD, Parkinson's disease; PI, propidium iodide; TRP, transient receptor potential; TRPM2, transient receptor potential melastatin 2.

1 | Introduction

The progressive death of dopaminergic neurons in the brain is a hallmark of Parkinson's disease (PD), the second most prevalent neurodegenerative disease [1]. The development of innovative medications and therapies is urgently required, as PD has emerged as a problem in the global medical sector [2]. Because PD is complicated and involves a variety of factors, its pathophysiology has not yet been fully understood. According to present literature information, the nigrostriatal dopaminergic neurons of the brain may sustain damage from excessive Ca^{2+}-influx-induced glutathione (GSH) depletion, mitochondrial (mROS), and cytosolic (cROS) reactive oxygen species [3, 4].

Ferroptosis, a type of cell death, has recently been identified and described in a variety of neurological disorders, including PD [5, 6]. The movement of Fe^{2+} between the mitochondria and the cytoplasm occurs normally in the body. When the mitochondrial dysfunction (mDYS), cytosolic iron free ion concentration ($c[Fe^{2+}]_c$) is disrupted, which ultimately results in ferroptotic apoptosis [7–9]. Thus, mDYS and the generation of high levels of mROS, which interfere with cytoplasmic and mitochondrial Fe^{2+} metabolism and ultimately cause ferroptosis and lipid peroxidation (LPO) in dopaminergic neurons, are main factors that contribute to the ferroptosis of PD [10–12]. In the neurons of PD, ferroptosis is also linked to an abnormal rise in the cytosolic free Ca^{2+} concentration ($c[Ca^{2+}]_c$) [13–15]. In a variety of disease models, excluding PD, several ferroptotic apoptosis cascades were induced by stimulating voltage-gated calcium channels (VGCC) and chemical-gated calcium channels (CGCC) [16–18]. Iron-dependent signaling and mROS are linked to the process of ferroptosis induction, which is demonstrated by the ferroptotic small molecules such as erastin (Erst) and RSL3 [9]. Erst promotes the formation of mROS by activating CGCC and VGCC and accelerating oxidation. Additionally, Erst disrupts the mitochondrial permeability transition pore, which increases apoptosis and mDYS [16–18]. One of the first synthetic antioxidants, ferrostatin-1 (Ferr1), is a selective inhibitor of ferroptosis that inhibits the synthesis of iron-dependent lipid hydroperoxide, lowers mROS and cROS levels, and successfully suppresses ferroptosis [19]. The most upstream participant in the ferroptosis pathway, the $c[Ca^{2+}]_c$ and cystine redox system, is suppressed when Ferr1, VGCC, and CGCC inhibitors are used [13–18]. It is well-documented that GSH facilitates the key regulatory function of glutathione peroxidase (GSH-Px) enzymes in ferroptosis. The cystine/glutamate antiporter system XC- (System XC-) converts glutamate into cystine, which is utilized to produce intracellular GSH [9]. Since cysteine is the rate-limiting component in GSH synthesis, Erst increased mitochondrial Ca^{2+} influx by inhibition of the cystine antiporter (System XC-) results in decreased GSH production [20]. Ferroptosis may result from the diminished antioxidant capability of the body and an accumulation of mROS [1–2]. The antioxidant response of microglia and SH-SY5Y cells with 1-methyl-4-phenylpyridinium (MPP)-induced parkinsonism is diminished when GSH levels are reduced through increased $c[Ca^{2+}]_c$, cytosolic ($c[Zn^{2+}]_c$) and mitochondrial ($m[Zn^{2+}]_c$) zinc ion accumulations-mediated mROS. This further raises mROS levels, which induce caspase-dependent apoptosis and cell death [22, 23]. However, its reduction through increased $c[Ca^{2+}]_c$-mediated mROS and caspase-independent (ferroptotic) cell death in SH-SY5Y cells with PD has not yet been studied. Excessive $c[Ca^{2+}]_c$-mediated mROS inhibits the activity of GSH-Px enzymes, particularly GSH-Px/4, which is a target of Erst and RSL3, and produces GSH depletion, both of which are essential periods upward of mDYS [23]. In rat neurons and SH-SY5Y cells, GSH treatment upregulated GSH-Px, which in turn reduced the transient receptor potential (TRP) cation channel stimulation (excessive $c[Ca^{2+}]_c$)-mediated mROS [22, 23].

TRP melastatin 2 (TRPM2) is an important member of the TRP main family, which also comprises a physiological sensor for ADP-ribose (ADPR) and oxidative stress [24, 25]. TRPM2 channel antagonists include 2-aminoethoxydiphenyl borate (2-APB) and N-(p-amylcinnamoyl)anthranilic acid (ACA) [26, 27]. TRPM2 was found to be involved in the genesis of PD in neurons and SH-SY5Y cells with MPP-induced parkinsonism [23, 28]. The SH-SY5Y cells and neurons with PD were found to have decreased GSH and GSH-Px levels but increased mROS, cROS, TRPM2 current densities, and cell death via TRPM2 channel stimulation-mediated Ca^{2+} and Zn^{2+} influx [26, 27]. While GSH therapy decreased TRPM2 activation in the cells with PD, GSH depletion increased it [23]. In gastric cancer cells, it was found that suppressing TRPM2 increased the ferroptosis caused by erastin and RSL3 [29]. The protective effects of TRPM2 inhibition on the regulation of oxidative stress, apoptosis, and death in PD-affected neuronal cells have not been investigated.

In the present study, we focused on the protective effects of antiferroptotics, including Ferr1 and GSH, on ferroptosis-induced increases in TRPM2 current density, oxidants (cROS, mROS, and LPO), cell death, Zn^{2+} ($c[Zn^{2+}]_c$ and $m[Zn^{2+}]_c$), and cytosolic free iron concentration ($c[Fe^{2+}]_c$) via TRPM2 activation but decreased GSH and GSH-Px in SH-SY5Y with PD (MPP). These factors have been found to be intermediary pathways in PD-mediated neurodegeneration.

2 | Materials and Methods

2.1 | Cell Culture

SH-SY5Y are neuroblastoma cells that express catecholaminergic markers and are capable of synthesizing dopamine. The TRPM2 channel in SH-SY5Y naturally exists, according to the expression results of earlier research [30, 31]. The neuronal MPP-induced parkinsonism model was employed in a number of investigations using the dopaminergic SH-SY5Y cells [28, 32]. Therefore, we employed SH-SY5Y cells (ATCC, Wesel, Germany) in the present investigation for two reasons. The mixture of DMEM and Hams' F12 medium with high glucose (4.5 g/L) is oxidant property, and it has TRPM2 stimulator action [33]. Hence, the SH-SY5Y cells were cultured in a cell culture medium mixture of DMEM (45%) and Ham's F-12 (45%) with low glucose (1 g/L) (Thermo Fisher Scientific, Istanbul, Türkiye) [32, 33]. To both medium combinations, 10% fetal bovine serum and 1% antibiotic mixture (penicillin/streptomycin) were added (Biochrom Ltd. Cambridge, United Kingdom). At a density of 1×10^7 cells per 25 cm^2 flask, the cells were grown in a sterile incubator (NB-203QS, Gyeonggi-do, Korea) at 37°C in a humidified environment with 5% CO_2.

2.2 | Study Groups

The six main groups in the SH-SY5Y cells were arranged as follows:

- The cells in the first group, known as the control (CNT), were cultured in the identical conditions and media for 24 h without receiving any treatments.
- The cell in the second (MPP) group was incubated with 0.5 mM MPP for 6 h [23].
- The cell in the third (MPP + Erst) group was incubated with 2.5 uM Erst for 24 h, and 0.5 mM MPP was added to the cells for the last 6 h of 24 h incubation [34, 35].
- The cell in the fourth (MPP + Erst + Ferr1) group was incubated with 2.5 μM Erst and 2 μM Ferr1 for 24 h [35, 36], and 0.5 mM MPP was added to the cells for the last 6 h of the 24 h incubation.
- In the fifth (MPP + Erst + GSH) group, the cells were incubated with 2.5 μM Erst for 24 h, and then 0.5 mM MPP (for last 6 h) and 10 mM GSH (for last two hours) were added to the cells.
- In the sixth (MPP + Erst + ACA) group, the cells were incubated with 2.5 μM Erst for 24 h, and then 0.5 mM MPP (for last 6 h) and 25 μM ACA or 100 μM 2-APB μM (for last hour) were added to the cells [23, 35, 36].

A ferroptosis is induced by the small molecule Erst, whereas ferroptosis is inhibited by the antioxidant Ferr1 [16–18]. In the present study, Ferr1 was employed to suppress ferroptosis, but we used Erst to induce ferroptosis. In the MPP + Erst group, we wished to test whether further stimulating ferroptosis with Erst would cause more TRPM2 activation and thus exacerbate MPP toxicity.

2.3 | $c[Ca^{2+}]_c$ Analyses

We measured changes in $c[Ca^{2+}]_c$ fluorescence intensity in the captured green images of cells using the laser scan confocal microscope (LSM 800, Zeiss, Oberkochen, Germany) after the 1 μM Fluo −3 AM (Calbiochem GmbH, Darmstadt, Germany) incubation [22, 23]. Fluo-3 AM at 488 nm was stimulated using argon lasers. At 527 nm, emission was maintained while excitation was maintained at 506 nm. The TRPM2 antagonist (100 μM 2-APB) was used to block Ca^{2+} entrance in SH-SY5Y prior to TRPM2 being stimulated by H_2O_2 (1 mM) in Fluo-3 AM investigations. We found that 2-APB had superior TRPM2 antagonist activity in previous Fluo-3 AM investigations [22, 23, 30] when compared to ACA. 2-APB was therefore employed to suppress TRPM2 in the cells.

2.4 | Electrophysiology

The EPC10 patch-clamp (HEKA GmbH, Lamprecht, Germany) was used to record the whole cell patch-clamp electrophysiological currents in the SH-SY5Y. The capillary resistance of the 1.5 mm borosilicate tube in the puller (PC-10, Narishige, Tokyo, Japan) was maintained between 4 and 8 MΩ, and the holding potential was maintained in the recordings at minus 60 mV. In the previous studies, patch chamber (extracellular) and patch pipette (intracellular) solutions have been described in detail [23, 24]. The osmolality of the buffers was maintained at 290 ± 30 mOsm. Instead of using Na^+, we employed N-methyl-D-glucamine ($NMDG^+$) to make a Na^+-free solution. TRPM2 is activated at high cytosolic Ca^{2+} concentration (1 μM) [37]. This resulted in a high calcium level in the intracellular buffer.

In the recordings, the TRPM2 channel was blocked by extracellular ACA (25 μM) and activated by cytosolic ADPR (1 mM). The current density results are displayed as pA/pF. The unit of pA/pF was calculated by dividing the cell capacitance (pF) by the highest current amplitude (pA) in SH-SY5Y.

2.5 | Cell Viability Percentage, Debris, and Cell Counts

The CASY Cell Counter + Analyzer Equipment Model TT electronic equipment (Roche Innovatis AG, Routlingen, Germany) measured the debris number (waste of dead cells), cell number, and cell viability changes in the SH-SY5Y cells using CASY tone solution. The analysis system uses an electronic probe system, and the cell viability result was displayed as a percentage of control, while the number of cells and debris numbers were given as $x10^7$ and $x10^6$ cells, respectively.

We used the colorimetric 3-(4,5-dimethylthiazol-2-yl)-2,5-diphenyltetrazolium bromide (MTT) test to repeat the cell viability analyses. The SH-SY5Y cells were studied in black 96-well plates at an initial density of 1×10^5 cells/well. After shaking the white 96-well plates for a minute, the absorbance in the quartz cuvette at 490 nm was measured using a spectrophotometer (UV-1800, Shimadzu, Kyoto, Japan). The MTT result was shown as a control percentage.

2.6 | PI Positive Cell Percentage Analyses

The blue color of the nucleus is represented by the Hoechst 33342 stain, which can enter the nucleus of a living cell. However, propidium iodide (PI) turns the nuclei of dying cells red. In the glass-bottom dishes, the SH-SY5Y was incubated with a combination of PI (2 μg/mL) (Cat # P1304MP, Thermo Fisher Scientific) and Hoechst 33342 (5 μM) (Cat # 4082, Cell Signaling Technology, Danvers, Massachusetts, USA) before the Axiocam 702 camera analysis. Using the ZEN blue software (Version 3.2) of Zeiss, the stained and captured images were analyzed under the CCD camera in the red (PI), blue (Hoechst), bright field (Black/white), overlay, and 2.5D formats. The emission wavelengths of PI/Hoechst were maintained at 617 nm/455 nm while excitation wavelengths of PI/Hoechst were maintained at 305 nm/348 nm. The total number of PI-positive cells was divided by the percentage of dead cells, which was then expressed as a percentage of PI-positive cells.

2.7 | Mitochondrial Dysfunction (mDYS), mROS, and cROS Assays

The amount of cROS in the cells was measured using the cROS probe (DCFH-DA, Cat #: C6827) (Thermo Fisher Scientific),

the LSM 800, and the plate reader (Infinite M200 microplate reader, Tecan, Mannedorf, Switzerland) [30, 32]. DCF is the fluorescent form of DCFH-DA when superoxide radicals are formed [38]. In the green DCF records of SH-SY5Y, which maintained the argon laser stimulation wavelength at 488 nm, the cROS studies employed excitation and emission wavelengths of 525 and 504 nm, respectively. Using the microplate reader (Infinite M200), the DCF fluorescence intensity in the cells was measured at 485 nm for excitation and 530 nm for emission.

The red fluorescent probe, MiSOX Red (Cat #: T7512), produces red fluorescence when it is oxidized by mitochondrial superoxide. An LSM 800 and 150 ng/mL of MiSOX Red dye were used to image the mROS generation of mitochondria, according to the manufacturer's instructions (Thermo Fisher Scientific). The red MitoSOX recordings were made with the argon laser stimulation wavelength set at 561 nm and the emission and excitation wavelengths set at 598 and 578 nm, respectively.

The mitochondria receive JC-1, a cationic carbocyanine dye [38]. The JC-1 probe (Cat #: T3168), according to the manufacturer (Thermo Fisher Scientific), generates an orange-fluorescent J-aggregate when mDYS in live cells becomes hyperpolarized. The JC-1 fluorescence in the SH-SY5Y was also measured with an LSM 800 and a plate reader. The images were produced using the excitation (593 nm) and emission (595 nm) wavelengths, while the orange JC-1 records were produced using the LSM 800 laser stimulation wavelength (488 nm). Additionally, the plate reader recorded changes in orange-fluorescent J-aggregate fluorescence.

In the plate reader analysis, the DCF and JC-1 results were shown as percentage changes (% of control), whereas the MiSOX, JC-1, and DCF were provided as arbitrary units (a.u.) in the LSM 800 experiments.

2.8 | $[Zn^{2+}]_c$ and GSH Imaging Analyses

Zn^{2+} labeling fluorescent dye (FluoZin-3 AM, Cat #: F24195, Thermo Fisher Scientific) was measured for $c[Zn^{2+}]_c$ and $c[Zn^{2+}]_c$. The mitochondria were tracked by using MitoTracker Red (MiTr) (Cat #: M7512, Thermo Fisher Scientific). The cells were exposed to 1 μM RhodZin3-AM and MiTr in dishes with a bottom glass for 15–20 min [39]. Following cell washing, the ZEN program of the Axiocam 702 camera was used to take red (MitoTr), green (FluoZin-3 AM), black/white bright field (BF), overlay, and 2.5D pictures of the probe inside the cells. The wavelengths of MiTr/FluoZin-3 AM for excitation and emission were kept at 578 nm/493 nm and 598 nm/513 nm, respectively.

ThiolTracker Violet GSH image detection reagent (Cat #: T10095) of manufacturer (Thermo Fisher Scientific) was used to measure the fluorescence of GSH present in the cells. The LSM 800 with a 40× oil objective was used to take the green pictures of ThiolTracker Violet in the cells. The ThiolTracker Violet recordings were made with the excitation, emission, and laser wavelengths set at 404, 526, and 405 nm, respectively.

2.9 | Cytosolic Free Iron Analyses

The $c[Fe^{2+}]_c$ was measured using FerroOrange (Cat #: F374, Dojindo, Japan). SH-SY5Y cells were cultured in the cell culture medium in glass-bottom dishes and stained with 1 μM FerroOrange for 30 min at 37°C in the dark. The LSM 800 was used to take the orange pictures (40× oil objective). The laser, emission, and excitation wavelengths of FerroOrange were maintained at 561, 575, and 551 nm, respectively. Using the ZEN blue software, the fluorescence intensity was assessed. The findings were displayed as a.u.

2.10 | The Determinations of LPO, GSH, and GSH-Px

The levels of lipid peroxidation (LPO) in the frozen SH-SY5Y cell samples were measured at 532 nm [40] using a UV-1800 spectrophotometer (Shimadzu, Kyoto, Japan). By comparing the absorbance to the standard curve of malondialdehyde equivalents that are produced when 1,1,3,3-tetramethoxypropane hydrolyzes in the presence of acid, the chemicals that are reactive to thiobarbituric acid reaction were quantified in the LPO analyses. The frozen cell samples were precipitated with 50% trichloroacetic acid and then centrifuged at 600×*g* for 6 min in order to perform the GSH measurement [41]. Tris-EDTA buffer (2.0 mL and 0.2 M, pH 8.9), cell supernatant (0.5), and 10 μM 5.5-dithiobis-2-nitrobenzoic acid (0.1 mL) were all present in the reaction mixture. After letting the solution reach room temperature for 5 min, the spectrophotometer (UV-1800) was used to measure it at 412 nm. GSH-Px activity of the frozen cell samples was determined by spectrophotometry at 412 nm and 37°C [42]. The stimulation of GSH-Px was performed in the analyses by using 1 mM cumene hydroperoxide. Lowry's reagent was utilized to determine the protein content of the cell homogenate samples in order to express the results as expressed per gram of protein. The LPO and GSH amounts are presented in μmol per gram of protein. GSH-Px activity is expressed in IU per gram of protein.

2.11 | Statistical Analyses

Group mean data were displayed as mean ± standard deviation STD. Tukey's post hoc test was followed by a one-way analysis of variance (ANOVA) in the SPSS software (25.0). A statistically significant result was defined as a significance value of $p < 0.05$.

3 | Results

3.1 | Treatments With GSH Reduced the Parkinsonism (MPP) and Erst-Induced Ferroptosis Increases in the Fluorescence Intensity of $c[Ca^{2+}]_c$ in the Cells Through TRPM2 Inhibition

The primary goal of this investigation is to determine whether exposure to ferroptosis (Erst) and parkinsonism (MPP) links to TRPM2 activation. This was accomplished by measuring $c[Ca^{2+}]_c$

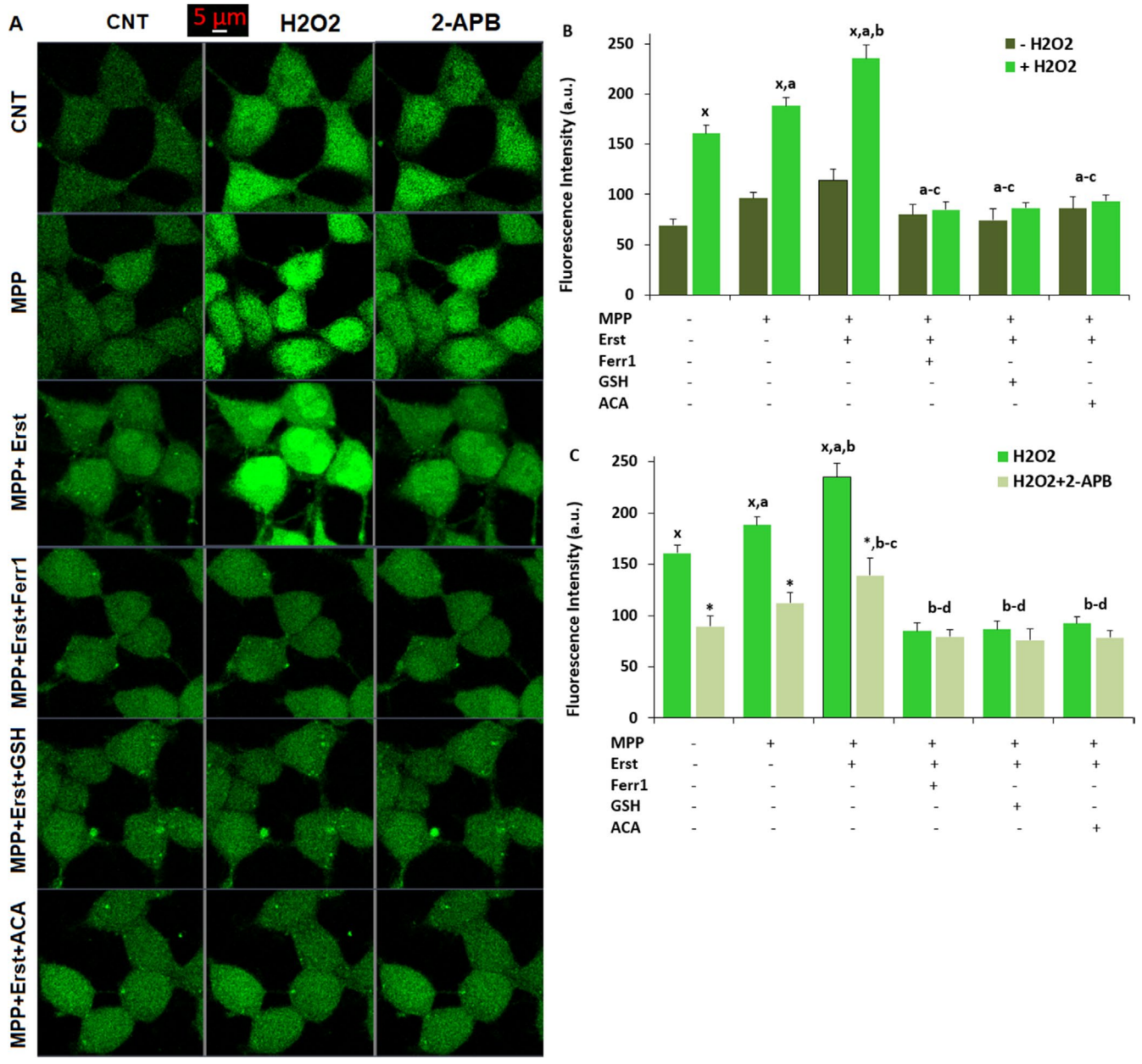

FIGURE 1 | GSH (10 mM for 2 h) reduced the PD (MPP) and ferroptosis-induced elevation of $c[Ca^{2+}]_c$ through inhibition of TRPM2 channel in SH-SY5Y cells. (mean ± STD). Fluo-3 AM (1 µM) was used for 40–50 min to stain the SH-SY5Y cells in each of the six groups (CNT, MPP, MPP + Erst, MPP + Erst + Ferr1, MPP + Erst + GSH, and MPP + Erst + ACA). Following the washing process, H_2O_2 (1 mM) stimulated TRPM2 in the cells, while 2-APB (100 µM) inhibited them. (A) displays representative images of six groups on the c[Ca2+]c through TRPM2 in the LSM 800 using a 40× oil objective. The $c[Ca2+]_c$ intensity changes of CNT ($-H_2O_2$) and H_2O_2 stimulated ($+H_2O_2$) cells were also shown by columns (B), although their changes in the H_2O_2 stimulated H_2O_2 + 2-APB cells were shown in (C). Five µm is a scale bar. From 8 to 10 cells in six-eight independent experiments for each condition. ($^a p < 0.05$ vs. CNT. $^b p < 0.05$ vs. MPP. $^c p < 0.05$ vs. MPP + Erst +2-APB. $^d p < 0.05$ vs. MPP + Erst. $^x p < 0.05$ vs. ($-H_2O_2$) group. $^* p < 0.05$ vs. (H_2O_2) group).

and analyzing the impact of the channel using both the TRPM2 agonist (H_2O_2) and the antagonist (2-APB). The $c[Ca^{2+}]_c$ fluorescence intensities were higher in the MPP than in the CNT, and they were even higher in the MPP + Erst group in the images (Figure 1A) and columns (Figure 1B,C). While 2-APB treatment (by TRPM2 inhibition) reduced the increases of $c[Ca^{2+}]_c$, H_2O_2 stimulation (by TRPM2 activation) further enhanced them in the CNT, MPP, and MPP + Erst groups ($p < 0.05$). In the MPP + Erst + Ferr1, MPP + Erst + GSH, and MPP + Erst + ACA groups, the fluorescence intensity of $c[Ca^{2+}]_c$ was lower than in the MPP and MPP + Erst groups ($p < 0.05$). The data unambiguously show how TRPM2-mediated Ca^{2+} influx functions in the PD model. Ferr1, GSH, and ACA treatments decreased the TRPM2-mediated elevation of $c[Ca^{2+}]_c$ in the MPP and MPP + Erst groups, as well as in the MPP + Erst + Ferr1, MPP + Erst + GSH, and MPP + Erst + ACA groups, according to the results.

3.2 | TRPM2 Current Density Was Elevated by ADPR Stimulation in MPP and MPP + Erst Cells but Not in Ferr1 and GSH-Treated Cells

In the second goal of the current investigation, we intended to further test the alterations using patch-clamp analysis in the SH-SY5Y cells in addition to the $c[Ca^{2+}]_c$ investigations. In the absence of ADPR stimulation of SH-SY5Y (Figure 2A), the TRPM2 current of cells remained unchanged. However, ADPR (1 mM) stimulation activated the TRPM2 of cells [Figure 2B (I-V)]. In the SH-SY5Y, the CNT + ADPR group had higher TRPM2 current densities as pA/pF (90,07) than the CNT group (5.23) (Figure 2J) ($p < 0.05$). By stimulating ADPR, the current density of TRPM2 in the cells was further ($p < 0.05$) increased in the Erst + ADPR group (152.52) [Figure 2C (I-V)], MPP + ADPR group (182.32) [Figure 2D (I-V)], and MPP + Erst + ADPR [Figure 2E (I-V)] (211.12). In comparison to the groups of CNT + ADPR and MPP + ADPR, the current density of TRPM2 in the cells was considerably ($p < 0.05$) lower in the CNT + ADPR + ACA/$NMDG^+$, MPP + ADPR + ACA/$NMDG^+$, and MPP + Erst + ADPR + ACA/$NMDG^+$ groups (Figure 2J). There was no increase in the TRPM2 currents following the ADPR stimulation by treating MPP + Ferr1 + ADPR (8.23) (Figure 2F), MPP + Erst + Ferr1 + ADPR (6.09) (Figure 2G), MPP + Erst + GSH + ADPR (7.09) (Figure 2H), and MPP + Erst + ACA + ADPR (Figure 2I), and they were lower ($p < 0.05$) in the groups as compared to the CNT + ADPR, MPP + ADPR, and MPP + Erst + ADPR. The patch-clamp findings further showed the protective function of GSH and the participation of TRPM2 in the parkinsonism (MPP) and ferroptosis-induced excessive Ca^{2+} influx in the neuronal cells.

3.3 | Treatments With GSH, Ferr1, and ACA Modulated MPP-Mediated Downregulation of Cell Viability and Cell Number Through the Downregulation of PI-Positive Cell Percentage and Debris Number

Several physiological and pathological processes, including ferroptosis, cell viability, and cell proliferation, are arranged by increases in $c[Ca^{2+}]_c$ in neurons caused by TRPM2 stimulation. Upon identifying the MPP-mediated increase in $c[Ca^{2+}]_c$ levels through TRPM2 activation, we suspected alterations in cell number, cell viability, MTT, debris number, and PI-positive death cell percentage, which is the third objective of the present study. MPP and MPP + Erst groups had lower ($p < 0.05$) cell viability (Figure 3A), MTT level (Figure 3B), and cell number (Figure 3C) than the CNT groups; however, their number and level were higher in the MPP + Erst + Ferr1, MPP + Erst + GSH, and MPP + Erst + ACA groups.

We obtained red/blue (PI/Hoechst), bright field (BF), overlay, and 2.5D images with the LSM 800 (Figure 4A). In the MPP and MPP + Erst groups, the debris number (Figure 3D) and PI-positive death cell percentage (Figure 4B) increased, but in the MPP + Erst + Ferr1, MPP + Erst + GSH, and MPP + Erst + ACA groups, their values decreased ($p < 0.05$).

3.4 | GSH, Ferr1, and ACA Treatments Reduced the MPP and Erst-Induced Elevations of Mitochondrial Oxidative Stress and Zn^{2+} Concentrations

There is growing evidence in SH-SY5Y cells that mDYS is caused by mitochondrial Ca^{2+} and Zn^{2+} accumulations [30, 32]. Thus, an increase in mDYS results in the production of mROS, cROS, and LPO [4, 7, 8, 11]. It has been shown that GSH modulates TRPM2, which in turn modulates the $c[Zn^{2+}]_c$ and $m[Zn^{2+}]_c$ increase-mediated induction of cROS in neurons [30, 32]. However, there is no evidence of how GSH modulates the oxidative neurotoxicity and TRPM2 activation caused by parkinsonism (MPP) and ferroptosis (Erst) through the accumulations of $c[Ca^{2+}]_c$ and $c[Zn^{2+}]_c$ in mitochondria in neural cells. We postulated that the MPP- and Erst-mediated increases in $c[Zn^{2+}]_c$, cROS, $m[Zn^{2+}]_c$, and mROS are caused by TRPM2 activation as the fourth goal of the present study. Red mROS (MiSOX), orange mDYS (JC-1), green cROS (DCF), overlay (Figure 5A), and 2.5D (Figure 5B) images were recorded in the cells. Red MiTr, green FluoZin-3, black/white bright field (BF), overlay, and 2.5D images were also recorded in the cells (Figure 6A).

The imaging results showed that the levels of mROS (Figure 5C), mDYS (Figure 5D,F), cROS (Figure 5E,G), LPO (Figure 5H), $c[Zn^{2+}]_c$ (Figure 6B), and $m[Zn^{2+}]_c$ (Figure 6C) ($p < 0.05$) were increased in the MPP group. Furthermore, mDYS, oxidants, and Zn^{2+} ($c[Zn^{2+}]_c$ and $m[Zn^{2+}]_c$) levels were further increased in the MPP + Erst group than in the MPP and CNT groups ($p < 0.05$). Additionally, we evaluated the modulator effects of the TRPM2 antagonist (ACA), anti-ferroptotic (Ferr1), and antioxidant (GSH) under MPP + Erst conditions on the mDYS, oxidants, and Zn^{2+} in the cells. The increases in mROS, mDYS, cROS, LPO, $c[Zn^{2+}]_c$, and $m[Zn^{2+}]_c$ were reduced by incubating GSH, Ferr1, and ACA ($p < 0.05$).

Our observations confirmed the function of ferroptosis (Erst) and parkinsonism (MPP) in oxidative neurodegeneration and $c[Zn^{2+}]_c$ buildup via TRPM2 activation in SH-SY5Y neuronal cells.

3.5 | GSH, Ferr1, and ACA Incubations Increased MPP and Erst-Induced Decreases of $c[Fe^{2+}]_c$ in SH-SY5Y Cells

The ferroptosis of PD is known to be primarily caused by increases in mDYS and mROS, which disrupt cytoplasmic Fe^{2+} metabolism and ultimately result in ferroptosis in dopaminergic neurons, including the human SH-SY5Y neuronal cell line [10–12]. We determined that the fifth objective of the current study would be to execute the $c[Fe^{2+}]_c$ in SH-SY5Y cells after seeing the rise in mDYS.

According to the FerrOrange imaging and 2.5D data (Figure 7A), when cells are treated with MPP, levels of $c[Fe^{2+}]_c$ increase ($p < 0.05$) (Figure 7B). Additionally, the MPP + Erst group had a greater $c[Fe^{2+}]_c$ than the MPP and CNT groups ($p < 0.05$). Furthermore, we assessed how the

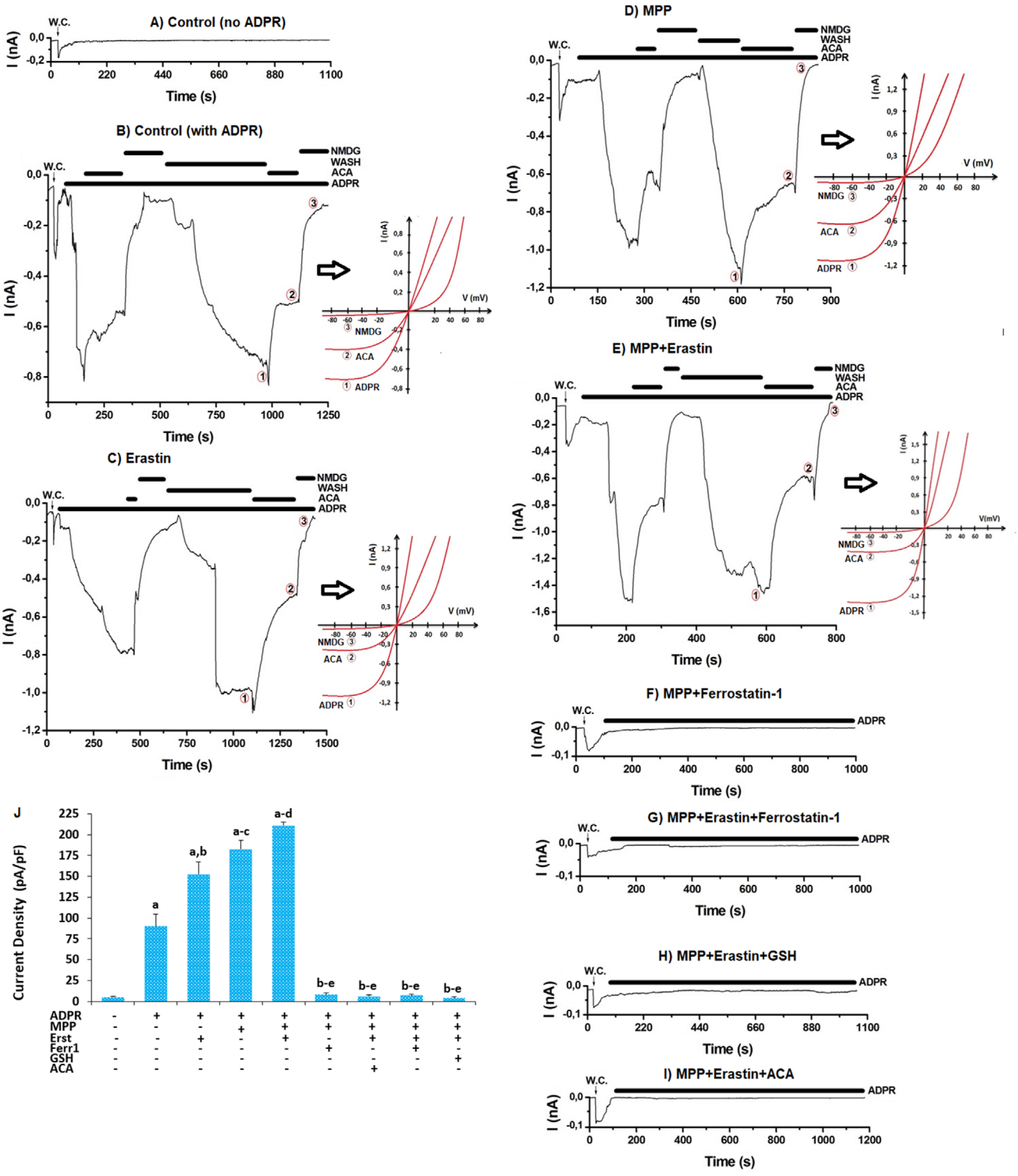

FIGURE 2 | Ferr1 (2 μM), GSH (10 mM), and ACA (25 μM) treatments reduced the TRPM2 current densities (pA/pF) induced by MPP (0.5 mM) and Erst (2.5 μM) in the SH-SY5Y cells. ($n = 3$ and mean ± STD). The cytosolic 1 mM ADPR (using a patch pipette) caused the TRPM2 currents in the SH-SY5Y cells, while extracellular ACA (25 μM) inhibited them. W.C.: The record of whole cell. (A) CNT (no ADPR). (B) CNT (ADPR). (C) Erastin (Erst) + ADPR. (D) MPP + ADPR. (E) Erst + MPP + ADPR. (F) MPP + Ferr1 + ADPR. Cells in the group were incubated by an MPP and Ferr1 combination before ADPR stimulation. (G) MPP + Erst + Ferr1 + ADPR. Cells in the group were incubated by an MPP, Erst, and Ferr1 combination before ADPR stimulation. (H) MPP + Erst + GSH + ADPR. Prior to ADPR stimulation, the group's cells were incubated with a combination of MPP, Erst, and GSH. (I) MPP + Erst + ACA + ADPR. The cells in the group were incubated with a mixture of MPP, Erst, and ACA before being stimulated by ADPR. (J) The mean TRPM2 current densities of groups. (C–E) showed the voltage ramps caused by ADPR, ACA, and $NMDG^+$ in the cells, indicated by the numbers 1, 2, and 3, respectively. ($^a p < 0.05$ vs. CNT without ADPR; $^b p < 0.05$ vs. CNT + ADPR group; $^c p < 0.05$ vs. MPP + ADPR group; $^d p < 0.05$ vs. Erst + ADPR group; $^e p < 0.05$ vs. MPP + Erst + ADPR group).

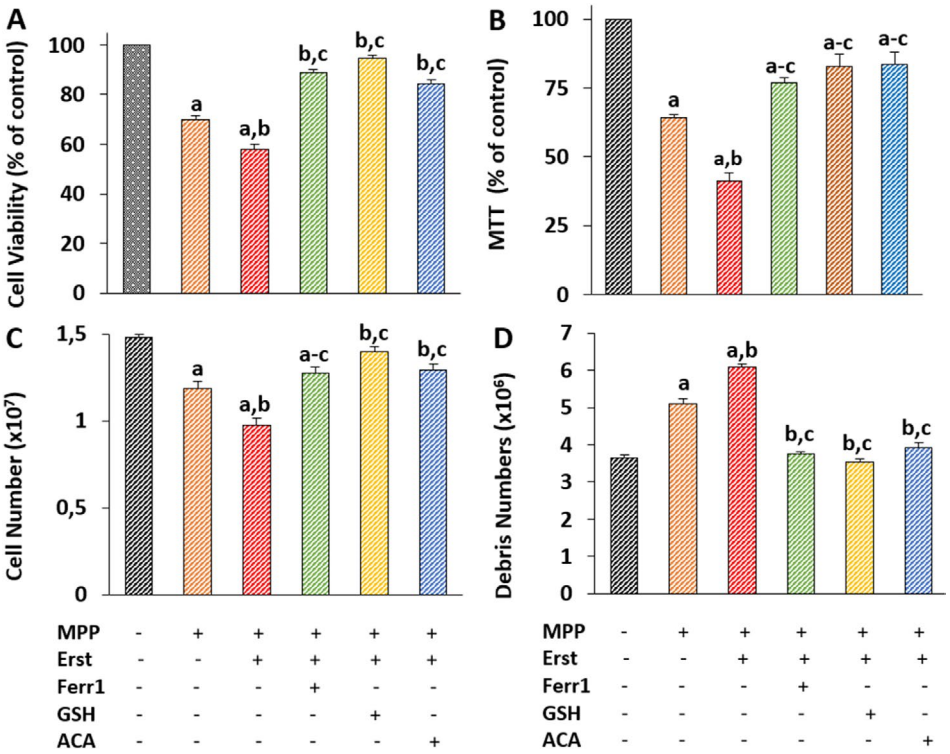

FIGURE 3 | The incubations of Ferr1 (2 μM), GSH (10 mM), ACA (25 μM) increased the PD (MPP) and Erst-induced ferroptosis decreases in cell number and viability. (Mean ± STD and $n = 3$). The SH-SY5Y viability (A), numbers (C), and debris (waste of dying cells) counts (D) were counted using the automated cell counter (CASY), although MTT (B) analysis were performed in the six group by using the spectrophotometer (UV 1800). ($^{a}p < 0.05$ vs. CNT. $^{b}p < 0.05$ vs. MPP group. $^{c}p < 0.05$ vs. MPP + Erst group).

TRPM2 antagonist (ACA), anti-ferroptosis (Ferr1), and GSH modulated the $c[Fe^{2+}]_c$ of cells under MPP + Erst conditions. Incubating GSH, Ferr1, and ACA decreased the increases in $c[Fe^{2+}]_c$ ($p < 0.05$).

3.6 | GSH, Ferr1, and ACA Incubations Increased MPP-Induced Decreases of GSH and GSH-Px in SH-SY5Y Cells

The increase of mROS stimulates the TRPM2 channel through the depletion of GSH and GSH-Px in SH-SY5Y cells, although GSH treatments inhibit TRPM2 stimulation in the parkinsonism (MPP) model [23] Treatments with Ferr1, GSH, and ACA cause VGCC in neuronal cells to be downregulated, which raises the amounts of GSH and GSH-Px [13–18]. We determine the levels of ThiolTracker violet (GSH) images (Figure 8A), GSH fluorescence intensity (Figure 8B), GSH levels (Figure 8C), and GSH-Px activity (Figure 8D) in the cells as the sixth goal of the current investigation. MPP considerably ($p < 0.05$) reduced the amounts of GSH fluorescence intensity, GSH levels, and GSH-Px activity in comparison to the CNT. Furthermore, compared to MPP alone, MPP + Erst further decreased GSH fluorescence intensity, GSH levels, and GSH-Px activity ($p < 0.05$). On the other hand, compared to the MPP and MPP + Erst groups, the treatment of GSH, Ferr1, and ACA considerably ($p < 0.05$) increased the concentrations of GSH and GSH-Px.

4 | Discussion

PD is a neurodegenerative disease that is relatively widespread in the aged population. It is characterized by a number of clinical symptoms, the most common of which is movement difficulties. One of the causes of PD, a complicated disease, is oxidative stress [1, 21]. Neuronal death and increased mDYS and mROS generation are caused by the buildup of $c[Ca^{2+}]_c$, $c[Fe^{2+}]_c$, and $c[Zn^{2+}]_c$ in mitochondria in MPP-induced parkinsonism [30, 32]. Ferroptosis results from a reduction in the antioxidant capacity of cells and the accumulation of mDYS-induced mROS, which causes iron deposition in the nigrostriatal region [9, 43]. Since PD triggers oxidative neuronal damage, there is growing evidence that TRPM2 activation plays a part in the pathogenesis of PD [28, 30]. Consequently, TRPM2 activation causes oxidative neuronal damage, whereas TRPM2 inhibition decreases both oxidative damage and PI-positive cell death. It has been demonstrated that TRPM2 channel blockers, such as GSH and ACA, decrease the amount of oxidative neurodegeneration produced by the TRPM2 activator (ADPR) in the microglia of mice [23] and the SH-SY5Y [28, 30, 32]. There is still confusion regarding how GSH, Ferr1, and ACA affect ferroptosis and oxidative stress caused by MMP and TRPM2 activation in SH-SY5Y cells (Figure 9). The present study observed that GSH, Ferr1, and ACA treatment decreased the effects of neuronal injury caused by PD (MPP) and ferroptosis (Erst) by upregulating antioxidants (GSH and GSH-Px) but downregulating oxidants (cROS, mROS, and LPO) and TRPM2 activity, PI-positive cell death percentage, $c[Ca^{2+}]_c$, $c[Fe^{2+}]_c$, and $c[Zn^{2+}]_c$.

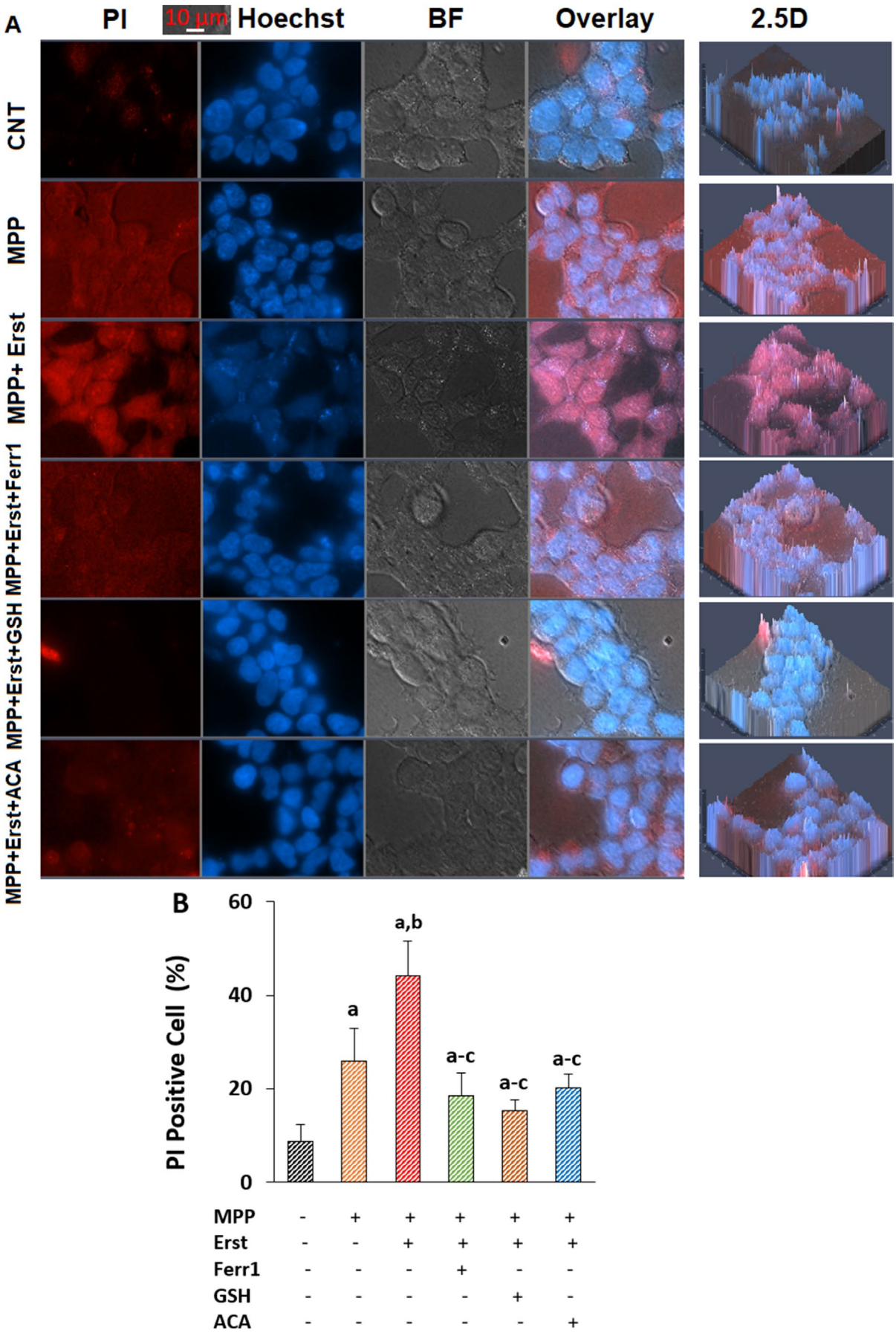

FIGURE 4 | Legend on next page.

FIGURE 4 | The treatments of GSH (10 mM for 2 h) modulated MPP and Erst-induced cell death through inhibition of ferroptosis and TRPM2. (Mean ± STD and $n = 6$). (A) The Axiocam 702 camera and inverted microscope (Axio Observer.Z1/7) were used to record the images of PI (red and dead cells), Hoechst (blue and live cells), bright field (BF and black/white), overlay, and 2.5D images. (B) The average percentage of PI-positive (cell death) cells among the six groups. (Objective: 40× oil. Scala bar: 10 μm). ([a]$p < 0.05$ vs. CNT. [b]$p < 0.05$ vs. MPP. [c]$p < 0.05$ vs. MPP + Erst).

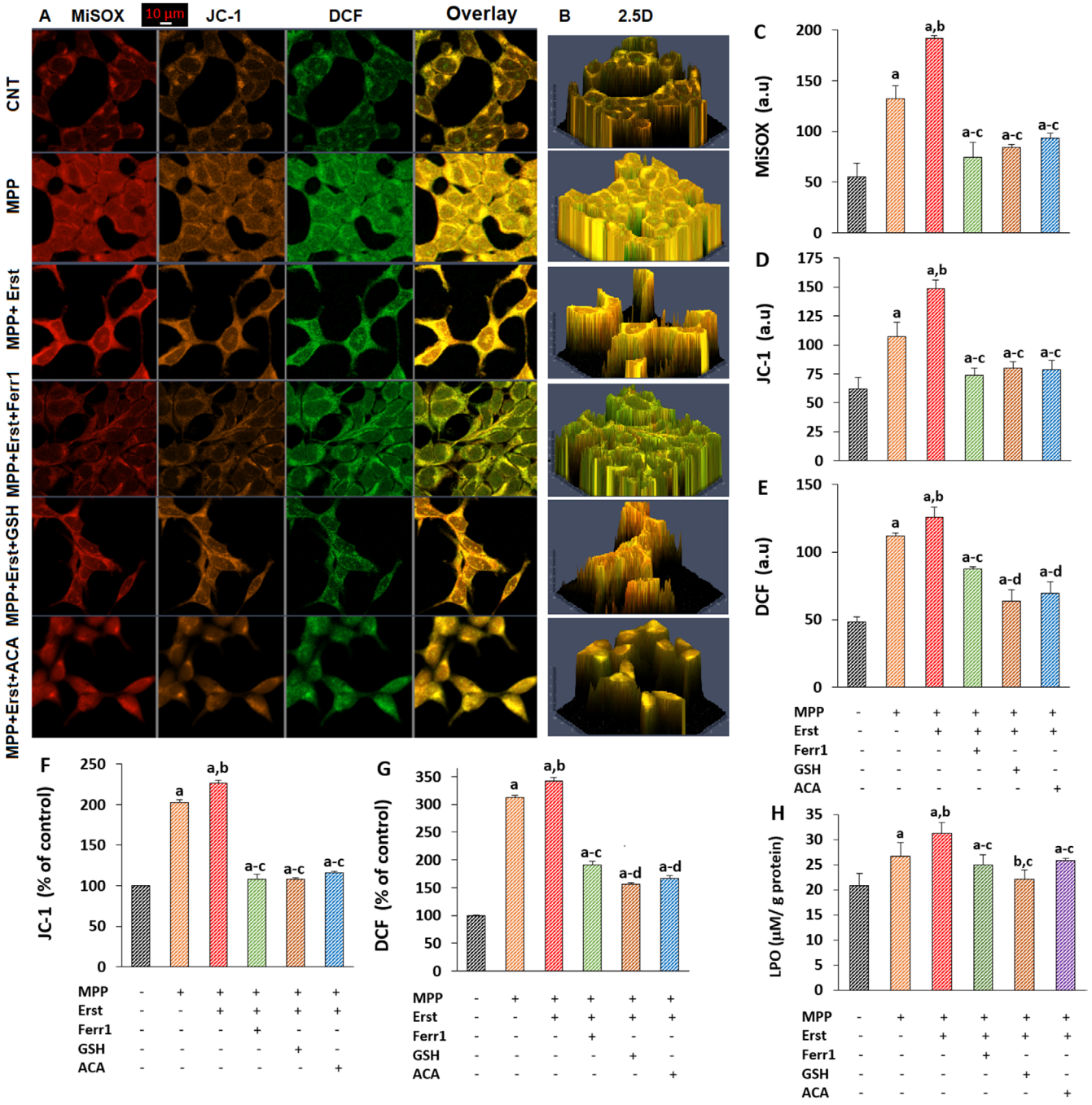

FIGURE 5 | The treatments of GSH (10 mM for 2 h) modulated MPP and Erst-induced increases of oxidative stress markers through inhibition of ferroptosis and TRPM2. (Mean ± STD and $n = 6$). (A) The red mROS (MiSOX), orange mDYS (JC-1), and green cROS (DCF) and 2.5D (B) images were captured in the LSM 800. The mean fluorescence intensities (arbitrary unit, a.u.) of MiSOX (C), JC-1 (D), and DCF (E) were shown by column graphics. The JC-1 (F) and DCF (G) analyses were repeated in the plate reader, and their fluorescence intensity changes were shown as % of control. (H) Lipid peroxidation (LPO) levels were determined in the cells by using the spectrophotometer (UV 1800). ([a]$p < 0.05$ vs. CNT. [b]$p < 0.05$ vs. MPP. [c]$p < 0.05$ vs. MPP + Erst. [d]$p < 0.05$ vs. MPP + Erst + Ferr1).

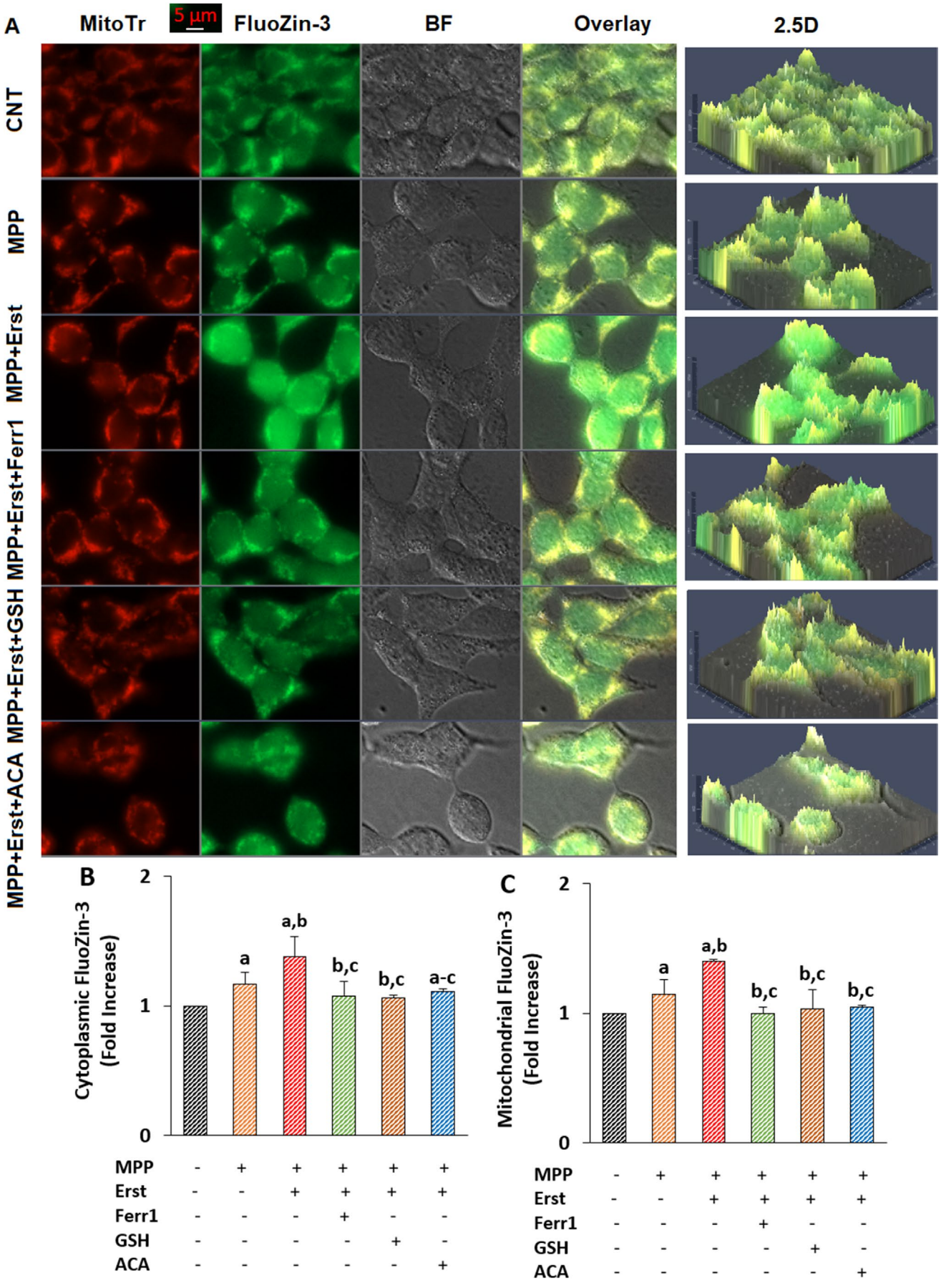

FIGURE 6 | Legend on next page.

FIGURE 6 | The GSH (10 mM) incubation modulated MPP (0.5 mM) and Erst (2.5 μM)-induced cytoplasmic ($c[Zn^{2+}]_c$) and mitochondrial ($m[Zn^{2+}]_c$) concentrations through inhibition of ferroptosis and TRPM2. (Mean ± STD and $n = 6$). (A) The images of MitoTracker Red (MitoTr), FluoZin-3 AM (red), bright field (BF and black/white), overlay, and 2.5D images were recorded in the Axiocam 702 camera. The fold increase (experiment/control) changes of $c[Zn^{2+}]_c$ (B) and $m[Zn^{2+}]_c$ (C) in the six groups. (Objective: 40× oil. Scala bar: 5 μm). ($^a p < 0.05$ vs. CNT. $^b p < 0.05$ vs. MPP. $^c p < 0.05$ vs. MPP + Erst).

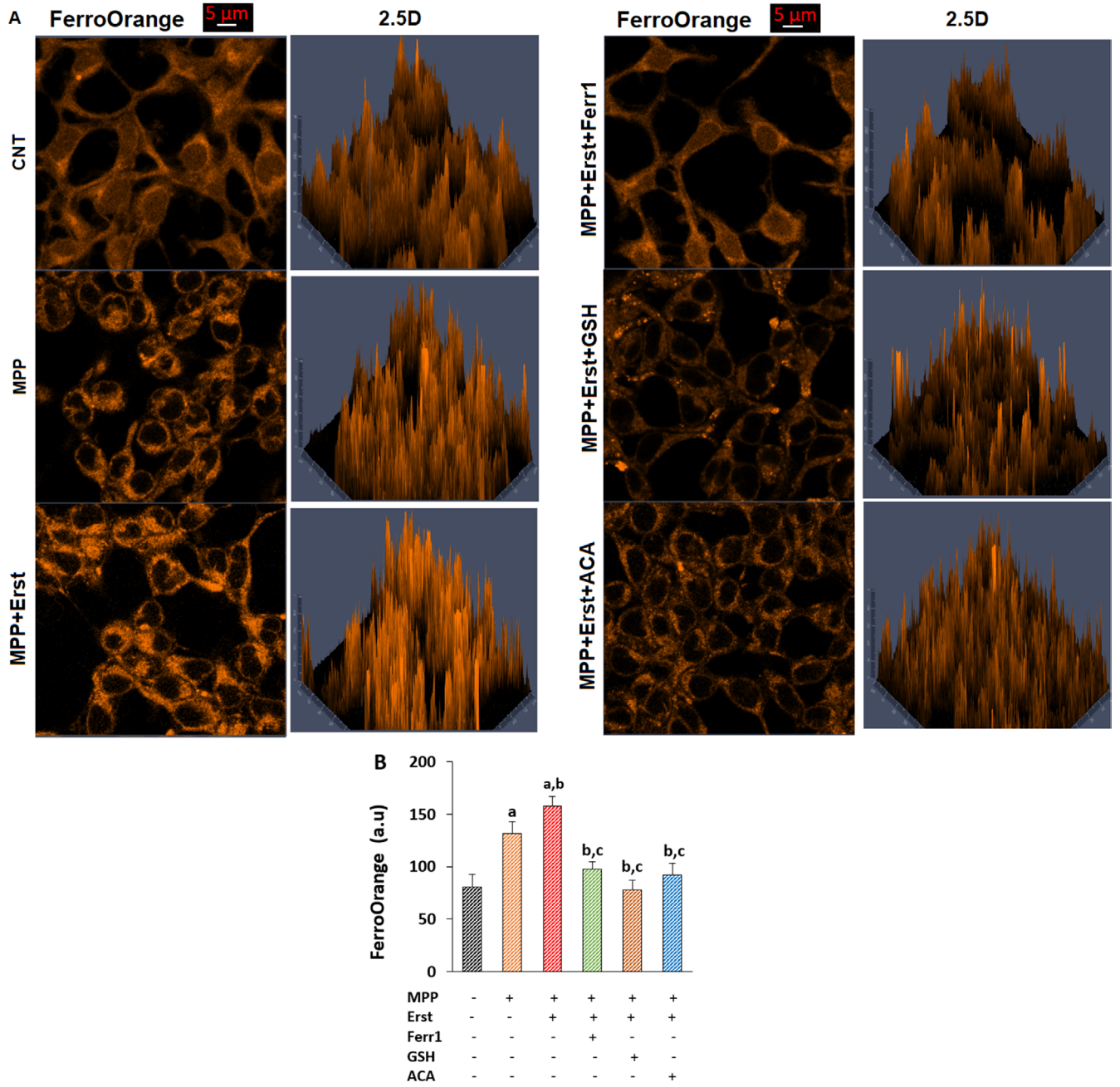

FIGURE 7 | The GSH (10 mM) incubation modulated MPP (0.5 mM) and Erst (2.5 μM)-induced cytoplasmic iron concentration ($c[Fe^{2+}]_c$) through inhibition of ferroptosis and TRPM2. (Mean ± STD and $n = 6$). (A) The images of FerroOrange and 2.5D images were recorded in the LSM 800. (B) The mean fluorescence intensities as arbitrary unit (a.u.) of $c[Fe^{2+}]_c$ in the six groups. (Objective: 40× oil. Scala bar: 5 μm). ($^a p < 0.05$ vs. CNT. $^b p < 0.05$ vs. MPP. $^c p < 0.05$ vs. MPP + Erst).

Stimulation of H_2O_2 production and poly (ADPR) polymerase (PARP)-1 activates TRPM2 in SH-SY5Y cells and neurons, generating ADPR and increasing TRPM2 current density and $c[Ca^{2+}]_c$ [28, 44, 45]. There is increasing evidence that GSH, TRPM2 antagonists (ACA and 2-APB), and PARP-1 inhibitors reduce the generation of cROS and mROS in PD-affected SH-SY5Y cells by reducing the H_2O_2-mediated increase of $c[Ca^{2+}]_c$ and ADPR-induced increase of TRPM2 current density

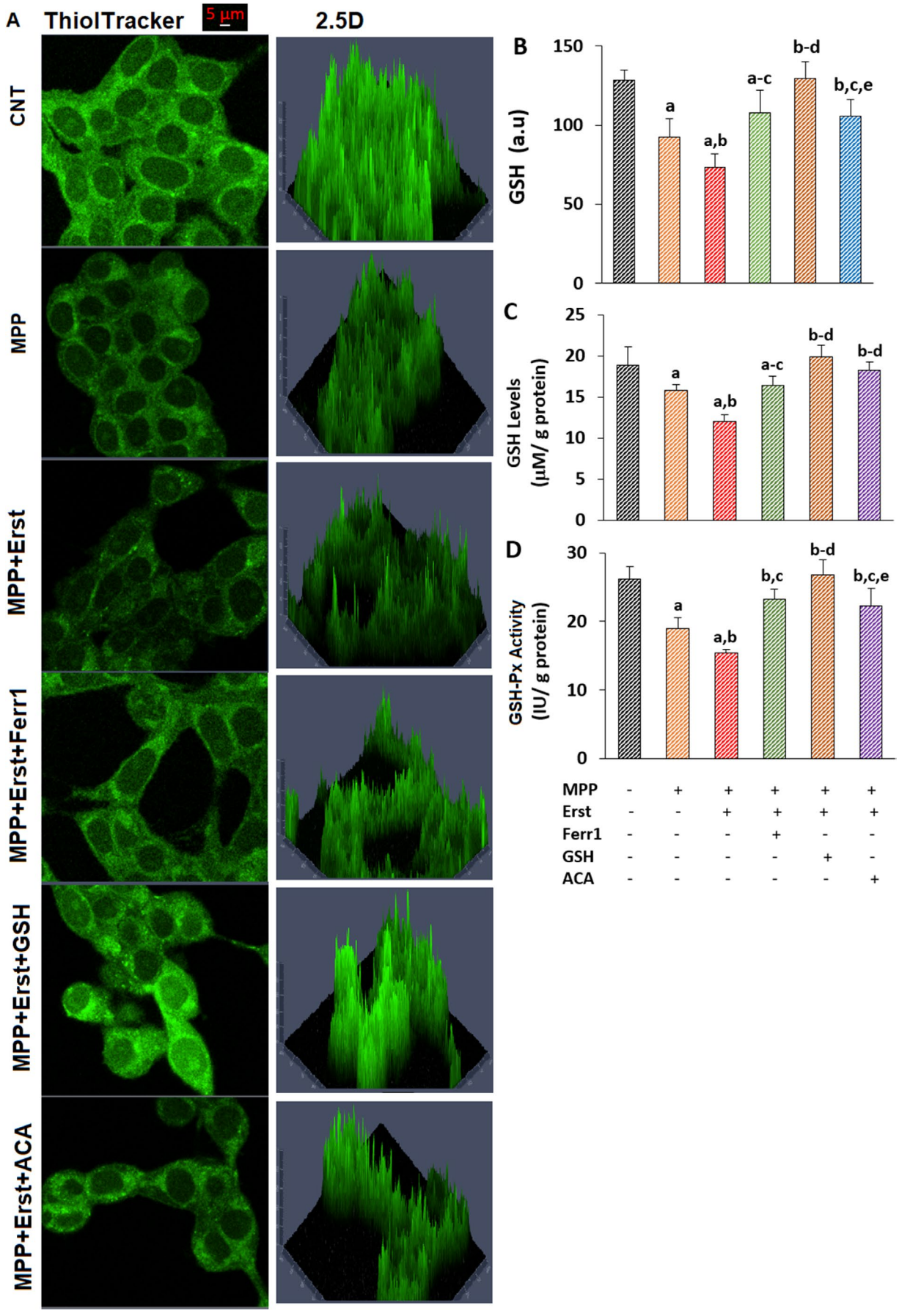

FIGURE 8 | Legend on next page.

FIGURE 8 | The MPP and Erst-induced decrease of GSH and GSH-Px was increased by the treatments of GSH, Ferr1, and ACA (mean ± STD and $n = 6$). The green cGSH (ThiolTracker Violet), and 2.5D (A) images were saved using the LSM 800 connected with a 40x oil objective, although GSH levels and GSH-Px activity were assayed in the spectrophotometer (UV-1800). A scale bar of 5 μm was maintained. Columns with an arbitrary unit (a.u.) of mean fluorescence intensity for ThiolTracker Violet fluorescence intensity (B), GSH levels (C), and GSH-Px activity (D). ([a]$p < 0.05$ vs. CNT. [b]$p < 0.05$ vs. MPP. [c]$p < 0.05$ vs. MPP + Erst. [d]$p < 0.05$ vs. MPP + Erst + Ferr1. [e]$p < 0.05$ vs. MPP + Erst + GSH).

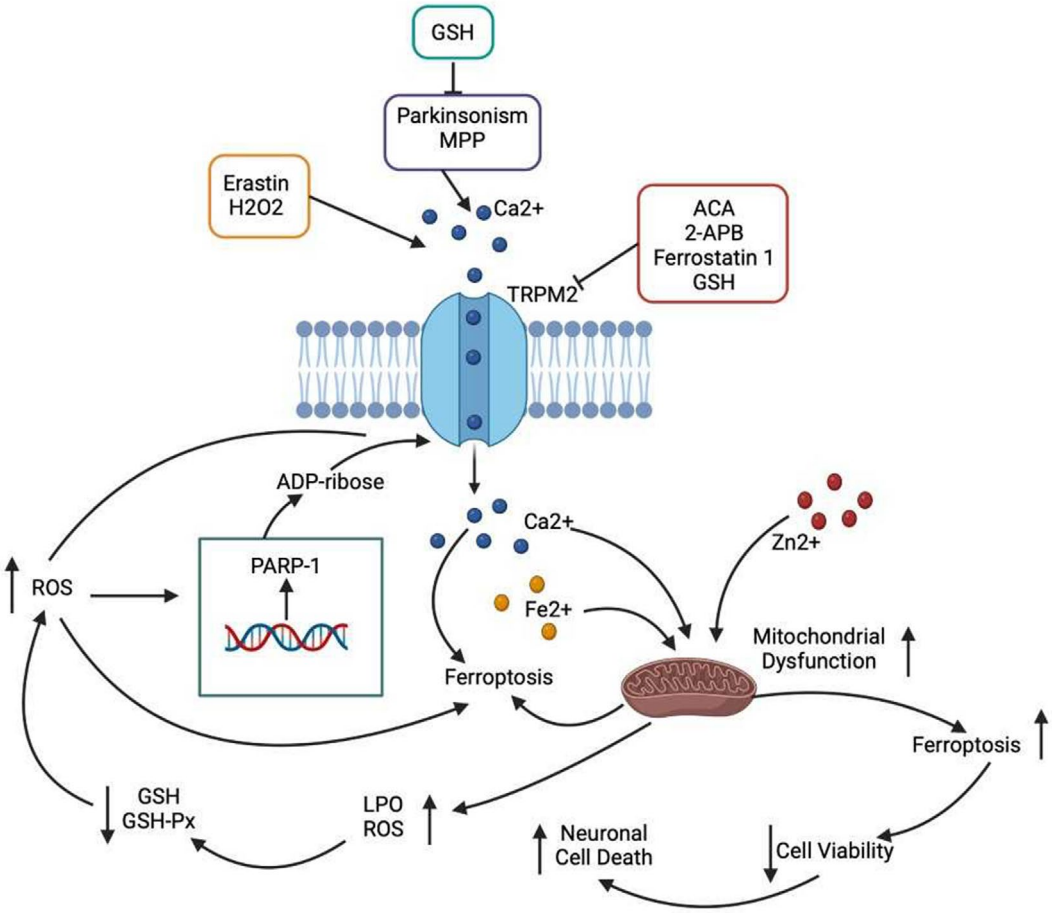

FIGURE 9 | Glutathione (GSH) diminishes parkinsonism (MPP)-induced ferroptosis and oxidative stress through the inhibition of the TRPM2 in neuronal cells. GSH protects the molecular pathways implicated in ferroptosis and oxidative stress by upregulating the GSH antioxidant system while suppressing TRPM2. TRPM2 is activated by oxidative stress and ADP-ribose, but it is blocked by ACA and 2-APB. The accumulation of free Ca^{2+}, Fe^{2+}, and Zn^{2+} into the mitochondria as a result of TRPM2 activation leads to an increase in mitochondrial membrane dysfunction. Cell death increased as a result of excessive mitochondrial ROS production and TRPM2 activation induced by Parkinson's disease (PD). Their oxidative activity, however, raises lipid peroxidation (LPO) while decreasing glutathione peroxidase (GSH-Px) activities and GSH levels. The increase in mitochondrial ROS caused by PD promotes DNA damage and the generation of ADPR by increasing the PARP-1 enzyme in the cell nucleus. Ferrostatin, ACA, 2-APB, and antioxidant GSH decrease TRPM2, which in turn affects oxidative neurodegenerative processes of PD.

[28, 30, 32]. GSH has been demonstrated to have antioxidant properties against the increases of oxidative damage and neuronal death but increases the decreases of neuronal numbers and cell viability caused by MPP and ferroptosis in the brains of mice and SH-SY5Y cells [14, 23, 36]. PARP-1 inhibitor treatments decreased oxidative damage and death in rat brain neurons by blocking TRPM2 [46]. Antioxidants have been shown to have neuroprotective and anti-ferroptotic effects by inhibiting PARP-1, promoting cell viability, cell number, GSH, and GSH-Px in PC12 neural cells [47]. When TRPM2 is activated, oxidants like cROS, mROS, and LPO increase. As a result, through activating TRPM2 in the SH-SY5Y cells, increased oxidative stress causes an excess of Ca^{2+} influx [28, 30, 32]. The present study showed that excessive oxidative stress generation and overloaded Ca^{2+} inflow in SH-SY5Y cells activated TRPM2, which in turn led to an increase in the $c[Ca^{2+}]_c$ and ADPR-mediated TRPM2 current densities in the parkinsonism (MPP) + ferroptosis (Erst) groups. The changes were higher in the MPP + erastin than in MPP only. Nevertheless, oxidative stress generation was decreased by antioxidants, GSH, Ferr1, and ACA, which also diminished the $c[Ca^{2+}]_c$ and ADPR-induced TRPM2 current densities in the cells.

In the previous experiments, the interaction between TRPM2 stimulation and GSH treatment was deeply investigated in different cells without ferroptosis. The GSH depletion increased

MPP-induced TRPM2 stimulation and oxidative stress changes, although GSH treatment decreased the changes in the microglia of mice. In the gastric cell line, TRPM2 knockdown reduced the concentration of GSH but enhanced the concentration of $c[Fe^{2+}]_c$, cROS, and LPO [23]. The GSH treatment decreased amyloid β42-induced increases of TRPM2 stimulation, LPO, and cROS in the hippocampus of wild-type mice but not in the TRPM2 knockout mice [48]. The cytosolic GSH depletion induced apoptosis and oxidative toxicity through TRPM2 stimulation in the hippocampus of aged mice [49]. Loss of GSH homeostasis associated with neuronal senescence facilitated TRPM2 activation in cultured hippocampal pyramidal neurons [50]. In the current study, we observed the TRPM2 channel blocker action of GSH in the parkinsonism (MPP) + ferroptosis (Erst) + GSH group. It seems that GSH treatment decreased the TRPM2 stimulation through the decrease of oxidative stress in the group. In the present study, we found that GSH had a TRPM2 channel blocker and antioxidant effects in the parkinsonism (MPP) + ferroptosis (Erst) + GSH group. By reducing oxidative stress in the group, GSH therapy appears to have reduced TRPM2 stimulation.

Low levels of GSH and GSH-Px, elevated concentrations of $c[Fe^{2+}]_c$, and oxidants such as LPO, cROS, and mROS produced during dopamine production are the primary causes of brain neuron death and neuronal viability in PD patients [6, 51]. GSH depletion or reduction will make people more vulnerable to oxidative stress, which can result in PD with or without increased TRPM2 stimulation [23, 48]. The huge amount of LPO is made when free radicals react with unsaturated fatty acids on the cell membrane. This can lead to lipid oxidation [3]. Prior research has demonstrated that mitochondrial activity is essential for ferroptosis [6–8]. Mitochondria are vital organelles in cells that primarily supply a significant quantity of energy by oxidatively phosphorylating the respiratory chain. Intensive Zn^{2+} accumulations and Ca^{2+} influx cause mitochondria to produce more oxidants and ferroptotic components [6–8, 44]. Prior research has demonstrated that MPP-induced increased TRPM2 stimulation-mediated neuronal death, mDYS, cROS, and mROS production via mitochondrial Zn^{2+} and Ca^{2+} upregulation in rodent microglia and SH-SY5Y cells, although these effects were influenced by GSH and TRPM2 antagonist incubations [28, 30, 32, 44]. TRPM2-induced neuronal death, mDYS, cROS, and mROS generation have not yet been examined in mouse neurons and cell lines exhibiting parkinsonism and ferroptosis. We investigated the effects of GSH, Ferr1, and ACA to find out whether oxidants (LPO, mROS, cROS, and mDYS) and accumulation-induced increases in cell death and ions ($c[Fe^{2+}]_c$, $c[Ca^{2+}]_c$, $c[Zn^{2+}]_c$, and $m[Zn^{2+}]_c$) were involved in MPP and Erst-induced increases of TRPM2 channel currents. GSH, Ferr1, and ACA downregulated the ion accumulations in SH-SY5Y cells, thereby totally blocking the rise of MPP and Erst-induced cell deaths and oxidants. The hypothesis of parkinsonism (MPP) without ferroptosis (Erst), however, is supported by these findings on mROS, cROS, and mDEP. This hypothesis suggests that MPP- and Erst-induced increases in Fe^{2+}, Zn^{2+}, and Ca^{2+} influxes into mitochondria raise mDYS, which in turn generates LPO, mROS, and cROS and causes cell death [28, 30, 32, 44].

The current data showed that the increase in mDYS was primarily associated with an increase in LPO and $c[Ca^{2+}]_c$ during BD and ferroptosis, while the decline in GSH and GSH-Px indicated that the injury to mitochondria in ferroptosis and MPP-induced oxidative neuron injury is primarily attributed to an increase in oxidants (mROS, cROS, and LPO) through TRPM2 activation. The oxidative neurodegenerative action of MPP and Erst returned following the incubations of GSH, anti-ferroptotic (Ferr1), and TRPM2 antagonist (ACA). GSH, Ferr1, and ACA treatments resulted in a decrease in the amounts of mROS, cROS, LPO, and $c[Ca^{2+}]_c$ in the mitochondria, whereas the GSH level and GSH-Px activity increased significantly. The antioxidant/oxidant balance through TRPM2 modulation is important for maintaining cell viability and antioxidant status [52]. The findings show that by modifying LPO and TRPM2-dependent Ca^{2+} influx, GSH, Ferr1, and ACA may raise the antioxidants (GSH and GSH-Px). Consistent with the current findings, GSH, Ferr1, and ACA therapy enhanced the MPP-induced reductions of GSH-Px and GSH concentrations in the mouse striatum, while the treatment decreased the concentration of LPO [53].

To summarize, the findings of this investigation have indicated that ferroptosis is influenced by TRPM2 stimulation in parkinsonism. GSH mitigates the damage to mitochondria and dopaminergic neurons caused by MPP through the TRPM2 signaling pathway. Additionally, it protects against mitochondrial damage, restores oxidative homeostasis in the MPP-exposed SH-SY5Y neuronal cells of parkinsonian models, inhibits the production of oxidants (mROS, cROS, and LPO), increases the content of free radical scavengers (GSH and GSH-Px), lowers the percentage of cell death and concentrations of ions ($c[Fe^{2+}]_c$, $c[Ca^{2+}]_c$, $c[Zn^{2+}]_c$, and $m[Zn^{2+}]_c$), and inhibits ferroptosis. In order to stop parkinsonism and ferroptosis-induced oxidative neurodegeneration and neuronal death, the current research suggests a unique treatment strategy that suppresses TRPM2 in neuronal cells.

Author Contributions

Elif Güzel: software, methodology, investigation, funding acquisition. **Ayşe Arzu Sayın Şakul:** writing – review and editing, validation, resources, funding acquisition. **Mustafa Nazıroğlu:** writing – review and editing, writing – original draft, validation, resources, methodology, formal analysis.

Acknowledgments

The authors wish to thank technicians (Fatih Şahin and Muhammad Şahin, BSN Health, Analysis and Innovation Ltd. Inc. Göller Bölgesi Teknokenti, Isparta, Türkiye) for helping with the analyses of the plate reader and patch-clamp. Elif Güzel used BioRender (www.biorender.com) to generate the graphical abstract (Figure 9).

Ethics Statement

The authors have nothing to report.

Consent

All authors reviewed the manuscript, and they approved submission of the manuscript. All authors have read and have abided by the statement of ethical standards for manuscripts submitted.

Conflicts of Interest

The authors declare no conflicts of interest.

Data Availability Statement

The data employed for supporting the present investigation's conclusions are accessible upon request from the corresponding author.

References

1. Y. Zilberter, D. R. Tabuena, and M. Zilberter, "NOX-Induced Oxidative Stress Is a Primary Trigger of Major Neurodegenerative Disorders," *Progress in Neurobiology* 231 (2023): 102539, https://doi.org/10.1016/j.pneurobio.2023.102539.

2. M. Li, H. Wang, Y. Bai, et al., "Pharmacodynamical Research of Extracts and Compounds in Traditional Chinese Medicines for Parkinson's Disease," *Fitoterapia* 177 (2024): 106086, https://doi.org/10.1016/j.fitote.2024.106086.

3. R. Tabassum and N. Y. Jeong, "Potential for Therapeutic Use of Hydrogen Sulfide in Oxidative Stress-Induced Neurodegenerative Diseases," *International Journal of Medical Sciences* 16, no. 10 (2019): 1386–1396, https://doi.org/10.7150/ijms.36516.

4. D. G. Lee, M. K. Kam, S. R. Lee, H. J. Lee, and D. S. Lee, "Peroxiredoxin 5 Deficiency Exacerbates Iron Overload-Induced Neuronal Death via ER-Mediated Mitochondrial Fission in Mouse Hippocampus," *Cell Death and Disease* 11, no. 3 (2020): 204, https://doi.org/10.1038/s41419-020-2402-7.

5. J. Wang, J. Zhao, K. Zhao, S. Wu, X. Chen, and W. Hu, "The Role of Calcium and Iron Homeostasis in Parkinson's Disease," *Brain Sciences* 14, no. 1 (2024): 88, https://doi.org/10.3390/brainsci14010088.

6. B. R. Stockwell, J. P. Friedmann Angeli, H. Bayir, et al., "Ferroptosis: A Regulated Cell Death Nexus Linking Metabolism, Redox Biology, and Disease," *Cell* 171, no. 2 (2017): 273–285, https://doi.org/10.1016/j.cell.2017.09.021.

7. S. K. Jang, S. H. Ahn, G. Kim, et al., "Inhibition of VDAC1 Oligomerization Blocks Cysteine Deprivation-Induced Ferroptosis via Mitochondrial ROS Suppression," *Cell Death and Disease* 15, no. 11 (2024): 811, https://doi.org/10.1038/s41419-024-07216-1.

8. L. P. Clemente, M. Rabenau, S. Tang, et al., "Dynasore Blocks Ferroptosis Through Combined Modulation of Iron Uptake and Inhibition of Mitochondrial Respiration," *Cells* 9, no. 10 (2020): 2259, https://doi.org/10.3390/cells9102259.

9. M. Figuera-Losada, A. G. Thomas, M. Stathis, B. R. Stockwell, C. Rojas, and B. S. Slusher, "Development of a Primary Microglia Screening Assay and Its Use to Characterize Inhibition of System xc- by Erastin and Its Analogs," *Biochemistry and Biophysics Reports* 9 (2017): 266–272, https://doi.org/10.1016/j.bbrep.2016.12.009.

10. F. Wang, X. Liu, M. Chen, et al., "Neuroprotective Role of CHCHD2 in Parkinson's Disease: Insights Into the GPX4-Related Ferroptosis Pathway," *Free Radical Biology and Medicine* 226 (2025): 348–363, https://doi.org/10.1016/j.freeradbiomed.2024.11.034.

11. X. Fu, L. Qu, H. Xu, and J. Xie, "Ndfip1 Protected Dopaminergic Neurons via Regulating Mitochondrial Function and Ferroptosis in Parkinson's Disease," *Experimental Neurology* 375 (2024): 114724, https://doi.org/10.1016/j.expneurol.2024.114724.

12. Z. Han, B. Wang, Y. Q. Wen, et al., "Acteoside Alleviates Lipid Peroxidation by Enhancing Nrf2-Mediated Mitophagy to Inhibit Ferroptosis for Neuroprotection in Parkinson's Disease," *Free Radical Biology and Medicine* 223 (2024): 493–505, https://doi.org/10.1016/j.freeradbiomed.2024.07.018.

13. P. Maher, K. van Leyen, P. N. Dey, B. Honrath, A. Dolga, and A. Methner, "The Role of Ca2+ in Cell Death Caused by Oxidative Glutamate Toxicity and Ferroptosis," *Cell Calcium* 70 (2018): 47–55, https://doi.org/10.1016/j.ceca.2017.05.007.

14. S. Zhang, Y. Geng, X. Jiang, et al., "Investigating the Mechanisms of Inflammation and Immune Alterations in Parkinson's Disease Using Spatial Transcriptomics Techniques," *Brain Research Bulletin* 217 (2024): 111076, https://doi.org/10.1016/j.brainresbull.2024.111076.

15. Y. Hirata, C. Yamada, Y. Ito, et al., "Novel Oxindole Derivatives Prevent Oxidative Stress-Induced Cell Death in Mouse Hippocampal HT22 Cells," *Neuropharmacology* 135 (2018): 242–252, https://doi.org/10.1016/j.neuropharm.2018.03.015.

16. S. Naderi, F. Motamedi, H. G. Pourbadie, et al., "Neuroprotective Effects of Ferrostatin and Necrostatin Against Entorhinal Amyloidopathy-Induced Electrophysiological Alterations Mediated by Voltage-Gated Ca2+ Channels in the Dentate Gyrus Granular Cells," *Neurochemical Research* 49, no. 1 (2024): 99–116, https://doi.org/10.1007/s11064-023-04006-7.

17. T. Wu, X. Wang, J. Cheng, et al., "Nitrogen-Doped Graphene Quantum Dots Induce Ferroptosis Through Disrupting Calcium Homeostasis in Microglia," *Particle and Fibre Toxicology* 19, no. 1 (2022): 22, https://doi.org/10.1186/s12989-022-00464-z.

18. I. Costa, D. J. Barbosa, S. Benfeito, et al., "Molecular Mechanisms of Ferroptosis and Their Involvement in Brain Diseases," *Pharmacology and Therapeutics* 244 (2023): 108373, https://doi.org/10.1016/j.pharmthera.2023.108373.

19. G. Miotto, M. Rossetto, M. L. Di Paolo, et al., "Insight Into the Mechanism of Ferroptosis Inhibition by Ferrostatin-1," *Redox Biolology* 28 (2020): 101328, https://doi.org/10.1016/j.redox.2019.101328.

20. C. H. Chang, H. X. Chen, G. Yü, C. C. Peng, and R. Y. Peng, "Curcumin-Protected PC12 Cells Against Glutamate-Induced Oxidative Toxicity," *Food Technology and Biotechnology* 52, no. 4 (2014): 468–478, https://doi.org/10.17113/ftb.52.04.14.3622.

21. M. Faysal, Z. Dehbia, M. Zehravi, et al., "Flavonoids as Potential Therapeutics Against Neurodegenerative Disorders: Unlocking the Prospects," *Neurochemical Research* 49, no. 8 (2024): 1926–1944, https://doi.org/10.1007/s11064-024-04177-x.

22. K. Yildizhan, R. Çinar, and M. Nazıroğlu, "The Involvement of TRPM2 on the MPP+-Induced Oxidative Neurotoxicity and Apoptosis in Hippocampal Neurons From Neonatal Mice: Protective Role of Resveratrol," *Neurological Research* 44, no. 7 (2022): 636–644, https://doi.org/10.1080/01616412.2022.2027644.

23. K. Yıldızhan and M. Nazıroğlu, "Glutathione Depletion and Parkinsonian Neurotoxin MPP+-Induced TRPM2 Channel Activation Play Central Roles in Oxidative Cytotoxicity and Inflammation in Microglia," *Molecular Neurobiology* 57, no. 8 (2020): 3508–3525, https://doi.org/10.1007/s12035-020-01974-7.

24. M. Nazıroğlu and A. Lückhoff, "A Calcium Influx Pathway Regulated Separately by Oxidative Stress and ADP-Ribose in TRPM2 Channels: Single Channel Events," *Neurochemical Research* 33, no. 7 (2008): 1256–1262, https://doi.org/10.1007/s11064-007-9577-5.

25. Y. Hara, M. Wakamori, M. Ishii, et al., "LTRPC2 Ca2+−Permeable Channel Activated by Changes in Redox Status Confers Susceptibility to Cell Death," *Molecular Cell* 9, no. 1 (2002): 163–173, https://doi.org/10.1016/s1097-2765(01)00438-5.

26. R. Kraft, C. Grimm, H. Frenzel, and C. Harteneck, "Inhibition of TRPM2 Cation Channels by N-(p-Amylcinnamoyl)anthranilic Acid," *British Journal of Pharmacology* 148, no. 3 (2006): 264–273, https://doi.org/10.1038/sj.bjp.0706739.

27. K. Togashi, H. Inada, and M. Tominaga, "Inhibition of the Transient Receptor Potential Cation Channel TRPM2 by 2-Aminoethoxydiphenyl Borate (2-APB)," *British Journal of Pharmacology* 153, no. 6 (2008): 1324–1330, https://doi.org/10.1038/sj.bjp.0707675.

28. Y. Sun, P. Sukumaran, S. Selvaraj, et al., "TRPM2 Promotes Neurotoxin MPP+/MPTP-Induced Cell Death," *Molecular Neurobiology* 55, no. 1 (2018): 409–420, https://doi.org/10.1007/s12035-016-0338-9.

29. D. Li, T. Wang, J. Lai, et al., "Silencing TRPM2 Enhanced Erastin- and RSL3-Induced Ferroptosis in Gastric Cancer Cells Through

Destabilizing HIF-1α and Nrf2 Proteins," *Cytotechnology* 74, no. 5 (2022): 559–577, https://doi.org/10.1007/s10616-022-00545-z.

30. Y. Akyuva and M. Nazıroğlu, "Resveratrol Attenuates Hypoxia-Induced Neuronal Cell Death, Inflammation and Mitochondrial Oxidative Stress by Modulation of TRPM2 Channel," *Scientific Reports* 10, no. 1 (2020): 6449, https://doi.org/10.1038/s41598-020-63577-5.

31. S. J. Chen, N. E. Hoffman, S. Shanmughapriya, et al., "A Splice Variant of the Human Ion Channel TRPM2 Modulates Neuroblastoma Tumor Growth Through Hypoxia-Inducible Factor (HIF)-1/2α," *Journal of Biological Chemistry* 289, no. 52 (2014): 36284–36302, https://doi.org/10.1074/jbc.M114.620922.

32. K. Yıldızhan and M. Nazıroğlu, "Protective Role of Selenium on MPP+ and Homocysteine-Induced TRPM2 Channel Activation in SH-SY5Y Cells," *Journal of Receptors and Signal Transduction* 42, no. 4 (2022): 399–408, https://doi.org/10.1080/10799893.2021.1981381.

33. H. Daldal and M. Nazıroğlu, "Carvacrol Protects the ARPE19 Retinal Pigment Epithelial Cells Against High Glucose-Induced Oxidative Stress, Apoptosis, and Inflammation by Suppressing the TRPM2 Channel Signaling Pathways," *Graefe's Archive for Clinical and Experimental Ophthalmology* 260, no. 8 (2022): 2567–2583, https://doi.org/10.1007/s00417-022-05731-5.

34. R. Zhou, Y. Chen, S. Li, et al., "TRPM7 Channel Inhibition Attenuates Rheumatoid Arthritis Articular Chondrocyte Ferroptosis by Suppression of the PKCα-NOX4 Axis," *Redox Biolology* 55 (2022): 102411, https://doi.org/10.1016/j.redox.2022.102411.

35. Y. Q. Wang, S. Y. Chang, Q. Wu, et al., "The Protective Role of Mitochondrial Ferritin on Erastin-Induced Ferroptosis," *Frontiers in Aging Neuroscience* 8 (2016): 308, https://doi.org/10.3389/fnagi.2016.00308.

36. L. Bai, F. Yan, R. Deng, R. Gu, X. Zhang, and J. Bai, "Thioredoxin-1 Rescues MPP+/MPTP-Induced Ferroptosis by Increasing Glutathione Peroxidase 4," *Molecular Neurobiology* 58, no. 7 (2021): 3187–3197, https://doi.org/10.1007/s12035-021-02320-1.

37. D. McHugh, R. Flemming, S. Z. Xu, A. L. Perraud, and D. J. Beech, "Critical Intracellular Ca2+ Dependence of Transient Receptor Potential Melastatin 2 (TRPM2) Cation Channel Activation," *Journal of Biological Chemistry* 278, no. 13 (2023): 11002–11006, https://doi.org/10.1074/jbc.M210810200.

38. D. C. Joshi and J. C. Bakowska, "Determination of Mitochondrial Membrane Potential and Reactive Oxygen Species in Live Rat Cortical Neurons," *Journal of Visualized Experiments* 51 (2011): 2704, https://doi.org/10.3791/2704.

39. K. Ertilav, "Neuroprotective Action of Honey Bee Venom (Melittin) Against Hypoxia-Induced Oxidative Toxicity and Cell Death via Inhibition of the TRPM2 Channel," *Journal of Cellular Neuroscience Oxidative Stress* 15, no. 3 (2023): 1162–1172, https://doi.org/10.37212/jcnos.1434545.

40. Z. A. Placer, L. L. Cushman, and B. C. Johnson, "Estimation of Product of Lipid Peroxidation (Malonyl Dialdehyde) in Biochemical Systems," *Analytical Biochemistry* 16, no. 2 (1966): 359–364, https://doi.org/10.1016/0003-2697(66)90167-9.

41. J. Sedlak and R. H. Lindsay, "Estimation of Total, Protein-Bound, and Nonprotein Sulfhydryl Groups in Tissue With Ellman's Reagent," *Analytical Biochemistry* 25, no. 1 (1968): 192–205, https://doi.org/10.1016/0003-2697(68)90092-4.

42. R. A. Lawrence and R. F. Burk, "Glutathione Peroxidase Activity in Selenium-Deficient Rat Liver," *Biochemical and Biophysical Research Communications* 71, no. 4 (1976): 952–958, https://doi.org/10.1016/0006-291x(76)90747-6.

43. M. Li, J. Zhang, L. Jiang, et al., "Neuroprotective Effects of Morroniside From *Cornus officinalis* Sieb. Et Zucc Against Parkinson's Disease via Inhibiting Oxidative Stress and Ferroptosis," *BMC Complementary Medicine and Therapies* 23, no. 1 (2023): 218, https://doi.org/10.1186/s12906-023-03967-0.

44. M. AlAhmad, H. Isbea, E. Shitaw, F. Li, and A. Sivaprasadarao, "NOX2-TRPM2 Coupling Promotes Zn2+ Inhibition of Complex III to Exacerbate ROS Production in a Cellular Model of Parkinson's Disease," *Scientific Reports* 14, no. 1 (2024): 18431, https://doi.org/10.1038/s41598-024-66630-9.

45. X. An, Z. Fu, C. Mai, et al., "Increasing the TRPM2 Channel Expression in Human Neuroblastoma SH-SY5Y Cells Augments the Susceptibility to ROS-Induced Cell Death," *Cells* 8, no. 1 (2019): 28, https://doi.org/10.3390/cells8010028.

46. B. Vaidya, H. Kaur, P. Thapak, S. S. Sharma, and J. N. Singh, "Pharmacological Modulation of TRPM2 Channels via PARP Pathway Leads to Neuroprotection in MPTP-Induced Parkinson's Disease in Sprague Dawley Rats," *Molecular Neurobiology* 59, no. 3 (2022): 1528–1542, https://doi.org/10.1007/s12035-021-02711-4.

47. G. Chen, C. Li, L. Zhang, et al., "Hydroxysafflor Yellow A and Anhydrosafflor Yellow B Alleviate Ferroptosis and Parthanatos in PC12 Cells Injured by OGD/R," *Free Radical Biology and Medicine* 179 (2022): 1–10, https://doi.org/10.1016/j.freeradbiomed.2021.12.262.

48. R. Çınar and M. Nazıroğlu, "TRPM2 Channel Inhibition Attenuates Amyloid β42-Induced Apoptosis and Oxidative Stress in the Hippocampus of Mice," *Cellular and Molecular Neurobiology* 43, no. 3 (2023): 1335–1353, https://doi.org/10.1007/s10571-022-01253-0.

49. İ. S. Övey and M. Naziroğlu, "Homocysteine and Cytosolic GSH Depletion Induce Apoptosis and Oxidative Toxicity Through Cytosolic Calcium Overload in the Hippocampus of Aged Mice: Involvement of TRPM2 and TRPV1 Channels," *Neuroscience* 284 (2015): 225–233, https://doi.org/10.1016/j.neuroscience.2014.09.078.

50. J. C. Belrose, Y. F. Xie, L. J. Gierszewski, J. F. MacDonald, and M. F. Jackson, "Loss of Glutathione Homeostasis Associated With Neuronal Senescence Facilitates TRPM2 Channel Activation in Cultured Hippocampal Pyramidal Neurons," *Molecular Brain* 5 (2012): 11, https://doi.org/10.1186/1756-6606-5-11.

51. N. Ballatori, S. M. Krance, S. Notenboom, S. Shi, K. Tieu, and C. L. Hammond, "Glutathione Dysregulation and the Etiology and Progression of Human Diseases," *Biological Chemistry* 390, no. 3 (2009): 191–214, https://doi.org/10.1016/10.1515/BC.2009.033.

52. M. Nazıroğlu, "New Molecular Mechanisms on the Activation of TRPM2 Channels by Oxidative Stress and ADP-Ribose," *Neurochemical Research* 32, no. 11 (2007): 1990–2001, https://doi.org/10.1007/s11064-007-9386-x.

53. Y. Qiu, Y. Cao, W. Cao, Y. Jia, and N. Lu, "The Application of Ferroptosis in Diseases," *Pharmacological Research* 159 (2020): 104919, https://doi.org/10.1016/j.phrs.2020.104919.